Dispersed Optical Heterodyne Detected Birefringence and Dichroism of Transparent Liquids

S. Constantine, Y. Zhou, J. Morais, and L. D. Ziegler*

Department of Chemistry, Boston University, Boston, Massachusetts 02215

Received: April 9, 1997; In Final Form: May 20, 1997[⊗]

The frequency-dispersed birefringence and dichroism of an electronically nonresonant liquid excited and probed by ultrafast pulses in an optically heterodyned detected configuration is reported. The nominally putative dichroic response of a transparent sample is shown to result from π out-of-phase contributions of Stokes and anti-Stokes third-order polarization components on, respectively, the red and blue sides of the probe pulse spectrum and are derived from CSRS and CARS type resonances. The strong corresponding nondispersed birefringent response, in contrast, results from the in-phase combination of these Stokes and anti-Stokes polarization components. Thus, by observing the dispersed probe pulse to the red or blue of the central carrier frequency, the various density matrix components, or pathways in time evolution history, contributing to either a dichroic or birefringent measurement may be more selectively viewed. The contribution of a particular nuclear response is enhanced when the observed frequency within the probe pulse spectrum is tuned to be either one quantum to the red or blue of the carrier frequency. This frequency-filtering technique can be used to enhance weak features in the total response, allow the determination of isotropic and anisotropic contributions to a nuclear response, and help probe the homogeneous and inhomogeneous character of the low-frequency Raman active density of states commonly observed in these two-pulse responses of nonresonant liquids. These effects are illustrated by the OHD birefringence and dichroism of $CHCl_3$.

Introduction

The analysis of the impulsively excited low-frequency responses of materials via the optically heterodyne detected (OHD) birefringence (optical Kerr effect) or dichroism is a well-established ultrafast spectroscopic method.[1−18] The observed electronic and nuclear responses can be described in terms of the third-order nonlinear polarization of the sample. By adjusting the phase of the local oscillator (LO), or read-out field, to be either $\pi/2$ out-of-phase or in-phase with the signal field, the real or imaginary part of the complex third-order polarization amplitude (P^3) controls the observed signal response.[1,9,10] These two responses are respectively known as the OHD birefringence or dichroism. This technique is essentially a standard femtosecond two-pulse experiment where the relative polarization orientations of all four fields involved in the pump−probe (or equivalently four-wave mixing) process have a particular well-defined relative orientation and the relative phase of the LO field is trivially controlled.[1−18] In the absence of a LO field, only a $|P^3|^2$ or homodyne signal is observed.[9,10] For transparent, i.e., electronically nonresonant materials, the OHD birefringent (Re P^3) response is much greater than the corresponding dichroic response (Im P^3). As previously described,[9] the relative magnitude of the nonresonant birefringence and dichroism results from the constructive and destructive interferences between the two density matrix time evolution histories that contribute to these responses. Furthermore, in the usual crossed polarizer configuration, the impulsively excited nuclear responses are proportional to the depolarized or anisotropic part (χ_{1221}) of the off-resonant inter- or intra-Raman scattering tensor.[9,10]

The goal of nonresonant femtosecond pulse OHD birefringence studies has generally been to probe the nature of intermolecular forces as revealed by the low-frequency responses of materials.[1−18] The Fourier transform of the OHD birefringence nuclear response, normalized by the pulse spectrum, is essentially equivalent to the low-frequency Raman spectrum.[9,10,18,19] Typically when ultrafast pulses are used to excite and probe the OKE of transparent liquids, Raman-active intramolecular modes on the order of the excitation bandwidth and a generally lower frequency nuclear response, associated with rotational reorientation and intermolecular degrees of freedom, are observed. The relative weightings of these various contributions to the nuclear response are determined by curve fitting and Fourier transform procedures.[4,5,7−17] Recently, OKE determined spectral densities have also been employed in calculations of electronically excited nuclear responses as observed by time dependent fluorescence Stokes shift[20] and photon echo[21] experiments.

In the studies reported here the probe pulse is dispersed and hence the time dependence of frequency-selected portions of the nonresonant birefringent or dichroic OHD responses are viewed. This allows the contributing density matrix pathways to be selectively observed. Consequently, in contrast to the total (nondispersed) OHD birefringence and dichroism of transparent materials, the frequency-dispersed dichroic response can be as large as the dispersed birefringent responses. As the detection frequency is tuned, the relative contribution of the different nuclear components to the OHD response can be controlled. Furthermore, since the nonresonant dichroic response can be easily observed by probe pulse dispersion, the relative polarization constraints of the standard OHD configuration can be relaxed, and thus both polarized and depolarized contributions to the system response can be observed (see below).

In a previous study[22] a frequency-resolved OHD dichroism of a nonresonant liquid, alternatively called forward impulsive stimulated Raman scattering (ISRS) in that report, was given for two wavelengths on the red and blue side of the transmitted probe pulse spectrum. However, we discuss and describe these observations in a different and more general context here. A third-order polarization treatment in a simple density matrix

[⊗] Abstract published in *Advance ACS Abstracts,* July 1, 1997.

S1089-5639(97)01227-9 CCC: $14.00

vibronic framework is given for the description of these frequency-selected nonresonant OHD birefringent and dichroic responses. In particular, this allows the four-wave mixing processes responsible for the generation of these new polarization components, their pulse frequency dependence and the relation between the birefringent and dichroic responses to be further characterized.

Frequency selected dichroic responses of electronically resonant samples, more commonly known as femtosecond pump−probe transient absorption spectra, are often reported and the effects of spectral filtering achieved by dispersing the probe pulse can often be quite pronounced.[23−30] Such frequency and time resolution allows the wave packet evolution on the excited-state surface to be observed. By proper choice of detection wavelength, the relative contribution of low-frequency intramolecular motions to the observed responses has been seen to be greatly enhanced as compared to the corresponding response observed when the total (integrated) probe beam is measured.[26,30]

The corresponding effects due to the observation of frequency-selected OHD responses of a nonresonant material is illustrated here by the birefringence and dichroism of chloroform. $CHCl_3$ has two low frequency (260 and 370 cm^{-1}) intramolecular Raman active modes as well as a lower frequency intermolecular Raman active spectral density. The nondispersed birefringence and dichroism of impulsively excited $CHCl_3$ has been previously reported.[9,10] Applications of this frequency dispersed technique, which include the enhancement of particular nuclear contributions to observed ground-state responses, the determination of isotropic as well as the anisotropic contributions to the low-frequency nuclear response, and the separation of homogeneous and inhomogeneous contributions to these liquid responses, are discussed below.

Experimental Section

The OHD birefringence and dichroism were obtained in the standard Kerr effect geometry with the sample and a quarter-wave plate placed between crossed polarizers.[1−18,31] 15 nm pulses (fwhh) with a pulse duration of ∼60 fs (Gaussian pulse assumed) centered at ∼800 nm from a Coherent Mira Ti: sapphire oscillator (76 MHz) were used to pump and probe these nonresonant responses. In-phase and $\pi/2$ out-of-phase local oscillators were obtained, respectively, by rotating the analyzing polarizer (after the sample) or input polarizer (before the quarter-wave plate) in the probe beam path. Samples were generally flowed through a 2 mm path length cell. Homodyne contamination of the OHD responses is removed by taking the difference between the two signed senses of the local oscillator field, i.e., differences between rotation directions of the polarizers. The probe pulse was dispersed by a 200 mm single (4 nm/mm linear dispersion) monochromator and detected by a photomultiplier tube. The pump pulse was chopped typically at 700 Hz, and the signal in the probe pulse direction was lockin (SRS 850) detected. The nondispersed responses shown here are obtained by setting the monochromator grating(s) to total reflection, i.e., a wavelength setting equal to zero.

It should be noted here that an alternative method for injecting an out-of-phase local oscillator for the observation of birefringent responses where the quarter-wave plate is rotated relative to the input polarizer has previously been employed[9,10] and was experimentally contrasted here with the above-described incident polarizer rotation scheme. The phases of the dispersed intramolecular mode contributions to the observed OHD birefringences of chloroform clearly revealed that when the quarter-wave plate was rotated relative to its fast axis, the observed response contained both dichroic and birefringent contributions. This was especially easy to discern in the dispersed OKEs, where responses on the red and blue sides of the probe pulse were observed. Only when the input polarizer before the quarter-wave plate is rotated are the expected phase relations (see below) obtained for the dispersed birefringent response across the pulse spectrum. The error introduced by this quarter-wave rotation method has been discussed previously in the context of nondispersed OHD measurements.[14,16]

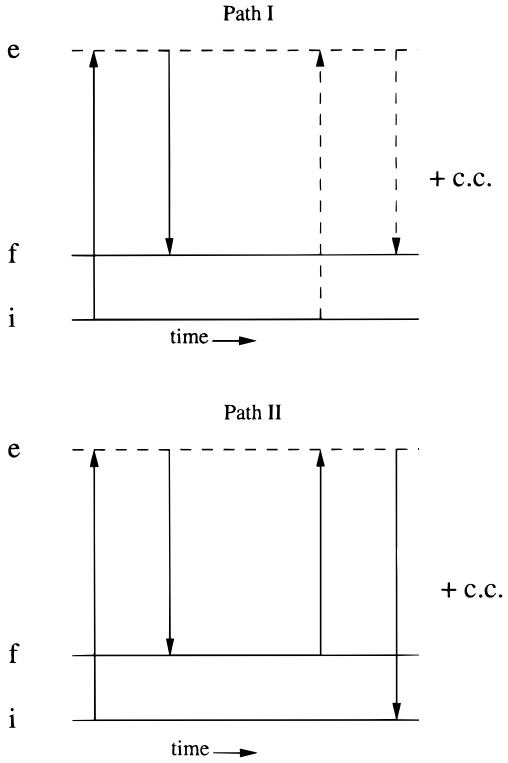

Figure 1. The two density matrix time evolution histories, labeled pathways I and II that contribute to the electronically nonresonant OHD birefringent and dichroic responses (within rotating wave and three-level approximations) are shown. Solid and dashed arrows correspond to bra and ket side matter−radiation interactions, respectively. Time is increasing from left to right. The initial, virtual (nonresonant intermediate), and final molecular levels are labeled i, e, and f, respectively.

Theory

The OHD pump−probe signal detected at frequency ω_2 and interpulse delay τ is given by[32]

$$S(\omega_2,\tau) = -2\ \mathrm{Im}\ \hat{E}^*_{\mathrm{LO}}(\omega_2)\,\hat{P}^3(\omega_2,\tau) \qquad (1)$$

where the spectrum of the local oscillator field centered at carrier frequency Ω is defined by

$$\hat{E}^*_{\mathrm{LO}}(\omega_2) = (1/\sqrt{2\pi})\int_{-\infty}^{+\infty} \mathrm{d}t\ \exp[-i(\omega_2 - \Omega)t]E^*_{\mathrm{LO}}(t) \qquad (2)$$

and the Fourier components of the third-order polarization field along the probe (k_2) direction are correspondingly

$$\hat{P}^3(\omega_2,\tau) = (1/\sqrt{2\pi})\int_{-\infty}^{+\infty} \mathrm{d}t\ \exp[i(\omega_2 - \Omega)t]P^3(k_2,t,\tau) \qquad (3)$$

The $P^3(k_2,t,\tau)$ response arising from an impulsively excited intra- or intermolecular Raman resonances on the ground electronic state surface may be viewed in a vibronic representation as arising from the contributions of two density matrix time evolution histories pictured in Figure 1.[9] Each vertical arrow represents a bra (solid) or ket (dashed) matter−radiation

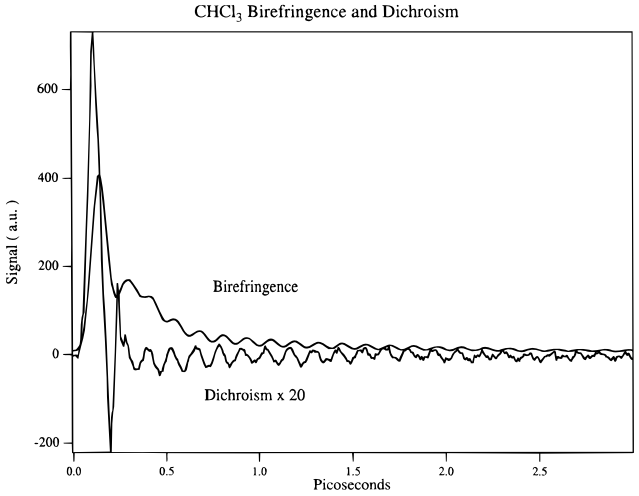

Figure 2. The total (nondispersed) birefringence and dichroism of $CHCl_3$ excited by 60 fs pulses centered at 799 nm. The intensity of the dichroism has been multiplied by a factor of 20.

interaction. Time is increasing from left to right. The number of possible time evolution histories considered here is restricted to paths I and II within a rotating wave approximation (RWA) and where all off-resonant intensity is ascribed to a single nonresonant level (three-level approximation). As already discussed,[9] path I is easily recognized as the density matrix time evolution history that contributes to nonresonant spontaneous Raman scattering (intensity level). In contrast, path II does not result in a net change of population in the material and thus contributes to coherent Raman scattering processes (CARS, see below) at an amplitude level description.

If we treat the ground-state vibrational resonance ($E_f - E_i = \omega_v$) as an exponentially damped (T_{2v}) decay, neglect the electronic dephasing of the nonresonant electronic level (e), and take the pulse to have a transform-limited Gaussian shape (fwhh $= 2\sqrt{\ln 2}\tau_p$), then the complex third-order polarization components at ω_2, and interpulse separation τ, for the two density matrix pathways are

$$\hat{P}^3_{I}(\omega_2,\tau) = -i\frac{\kappa}{\Delta^2}e^{i\omega_v\tau}e^{-\tau/T_{2v}}G(\Omega - \omega_v - \omega_2) \quad (4a)$$

$$\hat{P}^3_{II}(\omega_2,\tau) = i\frac{\kappa}{\Delta(\Delta - \omega_v)}e^{-i\omega_v\tau}e^{-\tau/T_{2v}}G(\Omega + \omega_v - \omega_2) \quad (4b)$$

κ is a constant that contains molecular transition moments and incident pump−probe field strengths and pulse widths, Δ is the off-resonance detuning from electronic resonance, $\omega_{ei} - \Omega$, and $G(\Omega \pm \omega_v - \omega_2)$ is a Gaussian defined by the Fourier transform

$$G(\Omega \pm \omega_v - \omega_2) = \int_{-\infty}^{\infty} dt \exp[-i(\Omega \pm \omega_v - \omega_2)t]e^{-t^2/2\tau_p} \quad (5)$$

where we have assumed that the pulse duration is shorter than the relaxation time of the nuclear coherence. Thus, $\hat{P}^3_{I}(\omega_2,\tau)$ and $\hat{P}^3_{II}(\omega_2,\tau)$ have contributions that respectively peak on the red and blue sides of the probe pulse spectrum. These OHD polarization components are generated by coherent Stokes (CSRS) and anti-Stokes (CARS) scattering-like processes[33] (see Figure 1) which are spatially overlapped as a result of the single pump beam impulsive excitation. In the usual continuous-wave CARS/CSRS configuration the ω_1 and ω_2 Fourier components come from different beams that overlap with some finite noncollinear angle in contrast to this experimental arrangement. The OHD dichroic and birefringent signals detected at ω_2 derived from each density matrix pathway are

$$S^{dic}_{I}(\omega_2,\tau) \propto \hat{E}_2(\omega_2)\mathrm{Im}\,\hat{P}^3_{I}(\omega_2,\tau) \propto \frac{\hat{E}_2(\omega_2)}{\Delta^2}G(\Omega - \omega_v - \omega_2)e^{-\tau/T_{2v}}\cos\omega_v\tau \quad (6a)$$

$$S^{dic}_{II}(\omega_2,\tau) \propto -\hat{E}_2(\omega_2)\mathrm{Im}\,\hat{P}^3_{II}(\omega_2,\tau) \propto -\frac{\hat{E}_2(\omega_2)}{\Delta(\Delta - \omega_v)}G(\Omega + \omega_v - \omega_2)e^{-\tau/T_{2v}}\cos\omega_v\tau \quad (6b)$$

$$S^{bir}_{I}(\omega_2,\tau) \propto \hat{E}_2(\omega_2)\,\mathrm{Re}\,\hat{P}^3_{I}(\omega_2,\tau) \propto \frac{\hat{E}_2(\omega_2)}{\Delta^2}G(\Omega - \omega_v - \omega_2)e^{-\tau/T_{2v}}\sin\omega_v\tau \quad (7a)$$

$$S^{bir}_{II}(\omega_2,\tau) \propto \hat{E}_2(\omega_2)\mathrm{Re}\,\hat{P}^3_{II}(\omega_2,\tau) \propto \frac{\hat{E}_2(\omega_2)}{\Delta(\Delta - \omega_v)}G(\Omega + \omega_v - \omega_2)e^{-\tau/T_{2v}}\sin\omega_v\tau \quad (7b)$$

$\hat{E}_2(\omega_2)$ is the probe pulse amplitude at ω_2. Thus, as previously described,[9] the relative phasing of the two density matrix pathway contributions to the nonresonant responses results in a dichroic signal which is 1−2 orders of magnitude weaker than the corresponding birefringence when the total integrated (all frequencies) pulse energy is observed. As eqs 6a,b reveal, pathways I and II modulate the probe pulse spectrum on the red and blue sides of the carrier frequency with π out-of-phase components (aside from a small energy denominator difference) for the dichroism. The contribution of these two polarization components Stokes and anti-Stokes to the carrier frequency are in-phase for the birefringence (eqs 7a,b). However, when the signal is frequency resolved, i.e., dispersed, the various pathways contributing to the nonresonant dichroism or birefringence may be independently observed. Consequently, both dichroic and birefringent response will exhibit nearly equal signal strength when these nonresonant polarization-dependent pump−probe signals are dispersed.

When the material's response is derived from a distribution of nuclear responses, the OHD signals are given by a sum of contributions of the type described above (eqs 6 and 7). Thus, a given mode's relative contribution to the OHD detected responses should be a maximum when detected at the vibrational frequency separation from the carrier frequency ($\omega_2 = \Omega \pm \omega_v$). Consequently, dispersed OHD birefringences/dichroisms provide a method for isolating or enhancing the contribution of distinct types of nuclear motion to these nonresonant responses and, potentially, helping to separate homogeneous and inhomogeneous contributions to the nuclear response function of transparent substances. It should also be noted, however, that these resonances will carry a width given by the probe pulse field spectrum.

Finally, the nonresonant dichroic response derived from a particular mode (eqs 6a,b) may be said to be due essentially to the pulse "wagging" to higher and lower frequencies. This qualitative description was given in an earlier analysis of nonresonant pump−probe responses.[22] In contrast, the corresponding birefringent response derives from the probe pulse energy at the detector increasing or decreasing at the frequency of the mode due to the pulse "broadening" resulting from the in-phase contributions of the CARS and CSRS polarization components (eqs 7a,b).

Results and Discussion

Comparison of Total and Dispersed Responses. The total, i.e., nondispersed, OHD birefringence and dichroism of $CHCl_3$

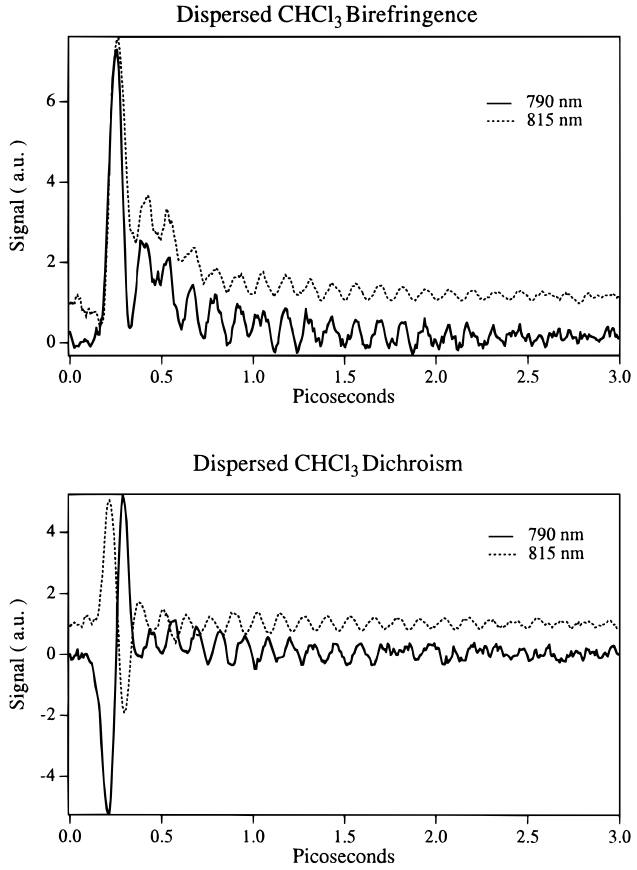

Figure 3. The dispersed birefringence and dichroism of $CHCl_3$ viewed at 790 and 815 nm (2 nm band-pass). These wavelengths are on the blue and red side of the probe pulse spectrum. The 815 nm responses are offset for clarity.

excited by 60 fs pulses centered at ~800 nm are shown in Figure 2. Intramolecular modes of 260 cm^{-1} (e) and 370 cm^{-1} (a_1), in addition to low-frequency intermolecular modes, contribute to this response as previously reported.[9,10] The contribution of the 260 cm^{-1} mode (128 fs period) dominates these responses beyond ~500 fs. As shown here and noted in other studies, the total birefringence is more than an order of magnitude larger than the corresponding nonresonant dichroic response.[1,9,10] Furthermore, in agreement with previous descriptions of OHD birefringence and dichroism,[9,10] a $\pi/2$ phase shift between the birefringent and dichroic responses is observed, and the low-frequency intermolecular modes are discriminated against in the dichroic response as seen in Figure 2.

In contrast to the total OHD responses (Figure 2), the dichroic and birefringent responses of $CHCl_3$ observed when only a portion of the probe pulse on the red and blue sides of the pulse spectrum are viewed are shown in Figure 3. The dispersed birefringence and dichroism of $CHCl_3$ observed at 815 and 790 nm (4 nm band-pass) are displayed in this figure. The contributions of the intramolecular modes to the birefringent responses on the red and blue side of the carrier frequency are clearly in-phase, while the corresponding contributions to the dichroic responses are π out-of-phase with respect to each other. Furthermore, the frequency-selected dichroic and birefringent responses exhibit a relative $\pi/2$ shift with respect to one another. These observations are consistent with the theoretical description given above (eqs 6 and 7). The usual total integrated dichroism and birefringence results from the sum of responses with these phase relationships across the entire pulse spectrum, and hence the birefringence dominates the nonresonant OHD pump−probe responses as compared to the corresponding dichroic signal.

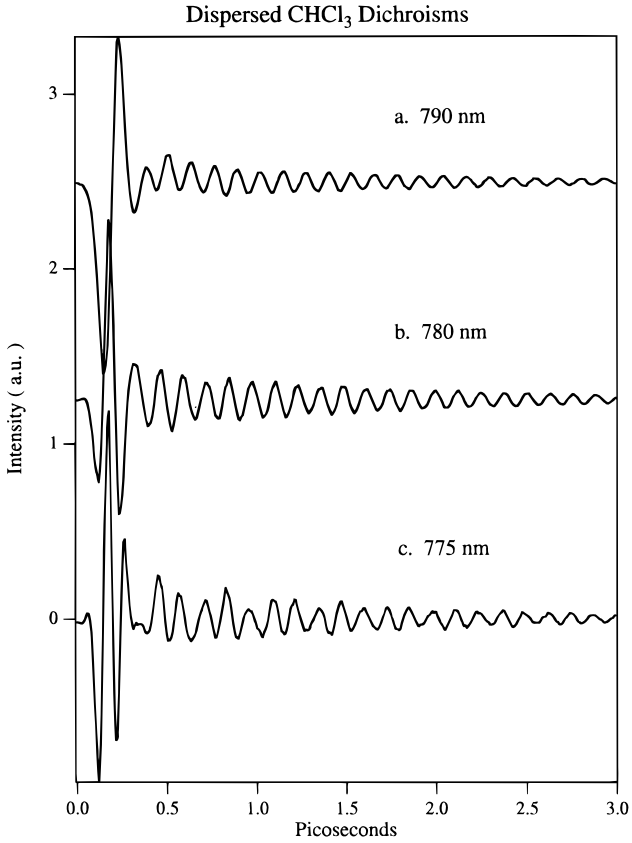

Figure 4. Dispersed dichroisms of $CHCl_3$ as a function of detection wavelength; 790, 780, and 775 nm. The dichroisms have been offset for clarity.

Frequency Filtering Effect. When the impulsively excited nuclear response contains contributions from several modes, the contribution from a given mode may be selectively enhanced by tuning the detection frequency to approximately a vibrational quantum spacing from the carrier frequency as the theoretical analysis above reveals (eqs 6 and 7). This effect is illustrated in Figure 4 for three detection wavelengths on the blue side of the probe pulse spectrum. As the monochromator is detuned further from the carrier frequency, the relative contribution of the 360 cm^{-1} mode to the 260 cm^{-1} mode increases as seen in the dispersed dichroic responses at 790, 780, and 775 nm (4 nm band-pass) and the corresponding power spectra shown in Figure 5. These wavelengths are detuned from the carrier (799 nm) by 140, 300, and 390 cm^{-1}, respectively. The same behavior is observed on the red side of the pulse spectrum.

A more dramatic example of this frequency-filtering effect and the potential of this frequency dispersed technique to more clearly expose components of the dichroism/birefringence that are not evident in the total responses is shown in Figure 6. The dispersed chloroform dichroism at 765 nm (bandwidth 4 nm; Figure 6) has a very different appearance than the previously displayed responses and, in particular, now shows evidence of a much higher frequency mode than the 360 cm^{-1} mode. The corresponding power spectrum, also shown in Figure 6, clearly shows an additional component at 668 cm^{-1}. This feature corresponds to a well-known strong totally symmetric Raman-active mode of $CHCl_3$.[34] It should be appreciated that this corresponds to an impulsively excited feature which is nearly 3 times the excitation bandwidth, and it is not observed in the singular value decomposition analyzed total (nondispersed) dichroism or birefringence of chloroform excited by even shorter (30 fs) pulses.[9,10,35] This example makes it clear that extremely

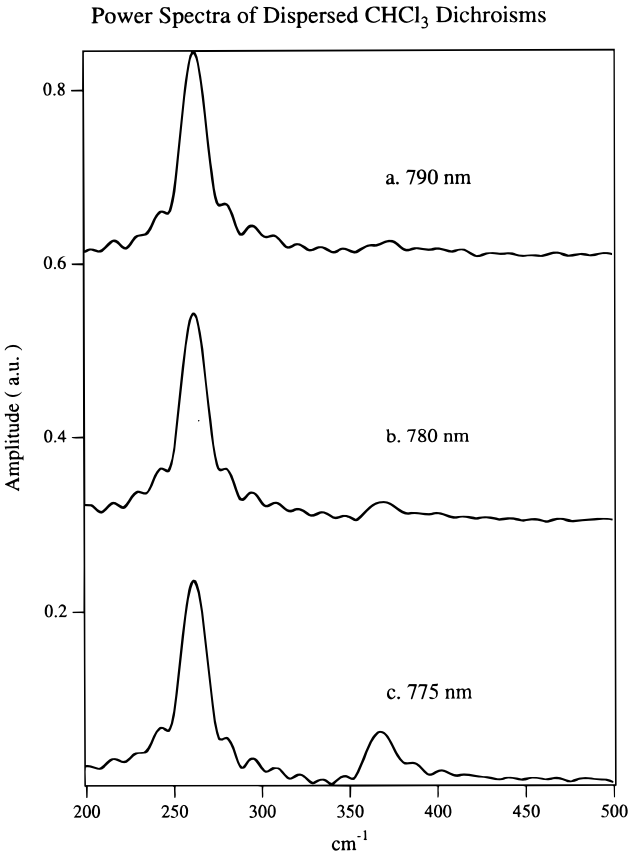

Figure 5. Power spectra of dispersed dichroisms of $CHCl_3$ shown in Figure 4. The power spectra have been offset for clarity.

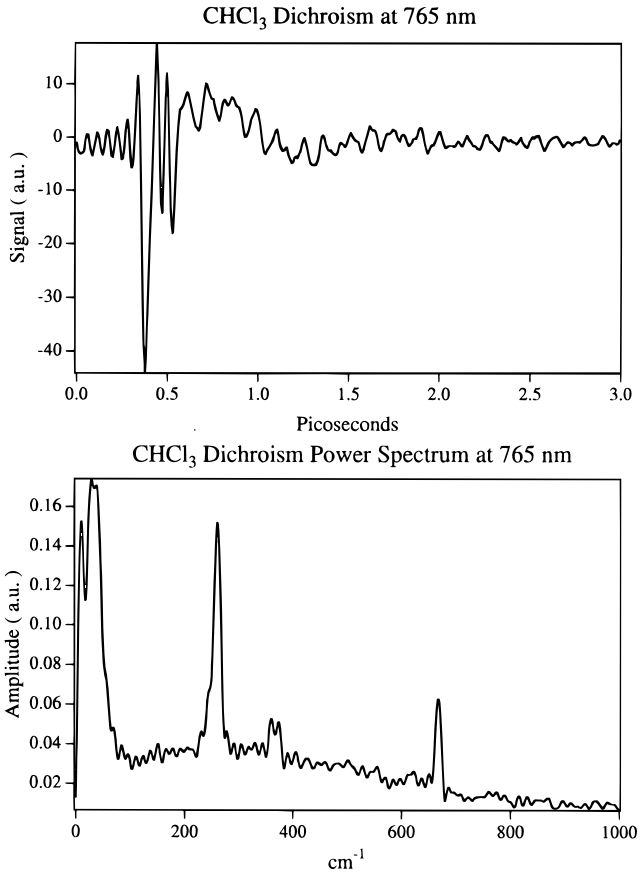

Figure 6. Dispersed dichroism of $CHCl_3$ cenetered at 765 nm and the corresponding power spectrum.

weak features virtually absent in a total birefringence (or dichroism) may be found or enhanced by this frequency-filtering technique.

This probe-dispersing effect is different from the so-called spectral filtering effect in OHD birefringence experiments described earlier[36] which is due to the finite bandwidth of the pump and probe pulses. The finite bandwidth/duration of the pump and probe will weight the relative amounts of different nuclear components to the observed responses and hence inherently "filter" the nuclear response. The pulse durations play the same role here as well. In addition, it should be noted that the finite probe bandwidth affects the resolution of spectral features as eqs 6 and 7 indicate.

Observation of Polarized (χ_{1111}) Component. Due to the crossed polarizer configuration normally employed to obtain OHD birefringence (dichroic) responses only the anisotropic (χ_{1221} or χ_{1122}) component of the Raman-active nuclear response contributes to the observed signals.[9,10] However, due to the inherent in-phase character of the dichroic local oscillator, the pump and probe beams can be oriented with any relative orientation in order to observe a dichroic response. When the polarization vectors of the pump and probe pulses have a parallel orientation only a very weak $CHCl_3$ dichroic response, which displays no obvious nuclear contributions, is obtained when the integrated probe beam is observed (see Figure 7). This response is obtained here by sending the probe pulse to the monochromator and tuning the monochromator wavelength setting to 0 nm, i.e., total reflection. Regardless of the relative polarization orientations of the pump and probe pulses an extremely weak dichroic response is obtained due to the cancellation of path-dependent polarization contributions on the red and blue side of the probe pulse as described above. However, when the monochromator is subsequently tuned to a wavelength within the probe envelope, the χ_{1111} response is readily obtained as

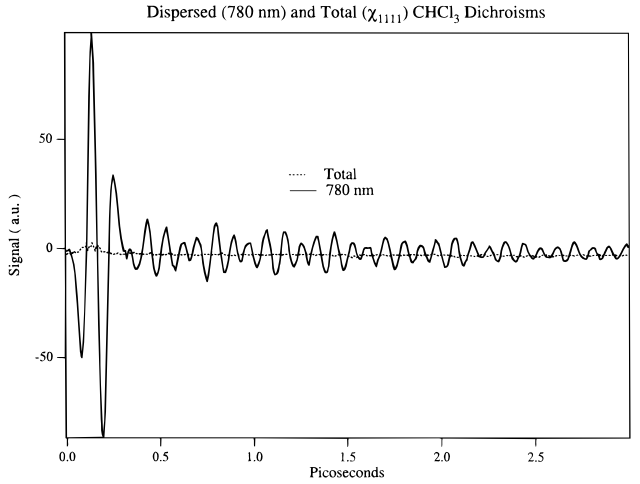

Figure 7. The total (nondispersed) and dispersed dichroisms of $CHCl_3$ centered at 780 nm.

demonstrated in Figure 7 by the chloroform dichroism detected at 780 nm. The signal is quite evident despite the necessarily large dc level it sits on in contrast to the typical near null background OHD experiments. Thus, one potential application of this method is that the polarized (χ_{1111}) as well as depolarized or anisotropic (χ_{1221} or χ_{1122}) scattering tensor elements may be observed via OHD dichroisms. In summary, this polarization flexibility is possible because the local oscillator does not have to be phase-shifted with respect to the probe pulse in order to observe nuclear responses via dichroic measurements, as required for the OHD birefringence measurements, and the dichroism is easily observed when frequency resolution is employed.

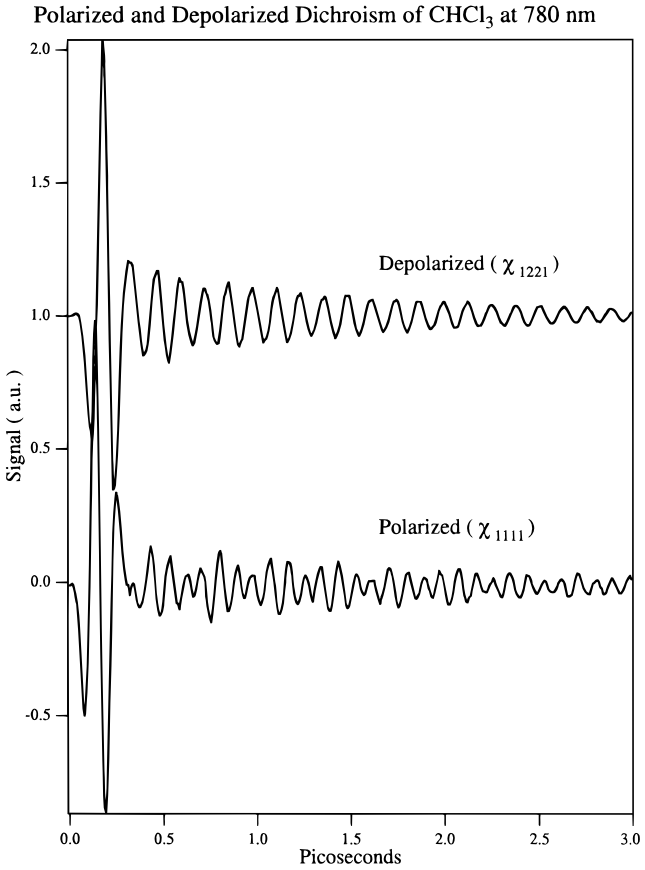

Figure 8. Comparison of polarized (χ_{1111}) and depolarized (χ_{1221}) dichroisms of $CHCl_3$ centered at 780 nm.

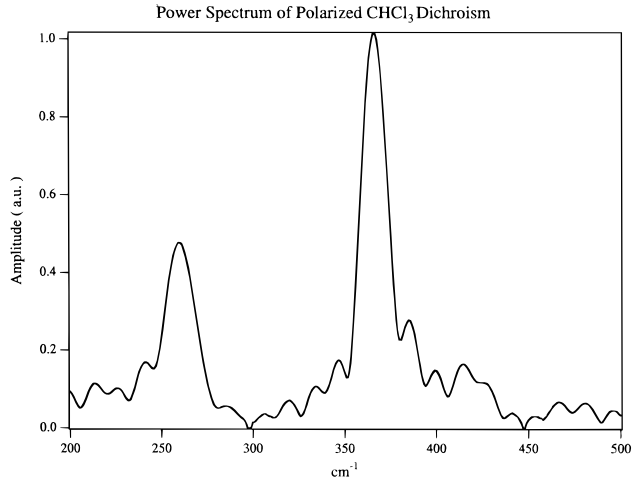

Figure 9. Power spectrum of polarized dispersed 780 nm dichroism of $CHCl_3$.

The χ_{1111} and χ_{1221} dichroic responses at 780 nm (4 nm bandpass) and the corresponding power spectra are compared in Figures8 and 9. As can be seen in these figures the 360 cm^{-1} is much more evident in the polarized (χ_{1111}) than the depolarized (χ_{1221} or χ_{1122}) signals as anticipated on the basis of the symmetry of these modes. The 260 and 360 cm^{-1} mode are respectively nontotally (e) and totally symmetric (a_1) modes.

Conclusions

The observed dispersed femtosecond OHD birefringence and dichroism of chloroform demonstrates the relative phasing of the path-dependent contributions to the total nonresonant responses. These responses are in agreement with the three-level, RWA density matrix description given here. The relative phasing of the third-order polarization components derived from CARS (red side) and CSRS (blue side) four-wave mixing processes, accounts for the large birefringent and weak dichroic response found for transparent materials in the usual nondispersed OHD configuration. The different density matrix pathways contributing to the OHD birefringence and dichroism can be selectively enhanced by frequency resolution of the probe pulse. By frequency resolving the probe beam in the dichroic configuration, dichroisms as large as birefringences are observed. This frequency "filtering" destroys the nearly perfect destructive interference that usually results in the putative dichroism of electronically nonresonant materials when the integrated probe energy is observed. The birefringent and dichroic signals may be said qualitatively to result from the "wagging" or "broadening", respectively, of the probe pulse spectrum at the frequency of the Raman-coupled nuclear motion.

The contribution of a particular nuclear motion to the OHD response can be enhanced by observing the dispersed response at a frequency detuned from the carrier frequency by the vibrational quantum of interest. This technique is shown here to allow observation of an impulsively excited nuclear response (668 cm^{-1}) at nearly 3 times the pulse bandwidth ($\sim$230 cm^{-1}) to be observed. Furthermore, since frequency resolution affords the measurement of the imaginary part of the complex P^3 amplitude via the transient dichroism, isotropic as well as anisotropic response functions may be determined as shown here by this frequency-filtering technique. This study also points out that although the solvent contribution to the dichroic response of a resonant solution (an electronically resonant chromophore in a transparent solvent) will generally not exhibit solvent contributions,[9] this may not be the case when frequency resolution is employed in a resonant pump−probe experiment.

However, probably the greatest opportunities afforded by this technique is to find or enhance nuclear response features not evident in a total birefringence of a transparent material and to address the issue of homogeneous or inhomogeneous contributions to the observed low-frequency responses. As has been discussed previously,[37,38] the decays of density matrix elements created at second order cannot by themselves be assigned to homogeneous or inhomogeneous character via pump−probe experiments since only one time interval is employed. However, when frequency resolution is added to these nonresonant two-pulse studies, the two-dimensional character of the observed responses may be viewed as a type of two-time probe interval technique. This principle is crudely demonstrated here where the relative amounts of the 260, 370, and 668 cm^{-1} modes of chloroform are shown to be dependent on the choice of probe pulse frequency. The frequency filtering undercuts the "inhomogeneous breadth" of the total nondispersed birefringent response at least due to the intramolecular responses. Studies exploiting this aspect of dispersed OHD dichroism and the observation and enhancement of weak or barely evident features in total birefringence of nonresonant samples, particularly with respect to the low-frequency Raman-active subspace, are currently underway. In addition, a more complete treatment of the dispersed nonresonant OHD responses which neglects the rotating wave approximation, treats finite temperature effects and includes more complicated vibrational response functions will be given elsewhere.

Acknowledgment. The support of the National Science Foundation (Grant No. CHE-9316148) and the Boston University Photonics Center are gratefully acknowledged.

References and Notes

(1) McMorrow, D.; Lotshaw, W. T.; Kenney-Wallace, G. A. *IEEE J. Quantum Electron.* **1988**, *24*, 443.
(2) Lotshaw, W. T.; McMorrow, D.; Kenney-Wallace, G. A. *Proc. SPIE* **1988**, *981*, 20.
(3) Kalpouzos, C.; McMorrow, D.; Lotshaw, W. T.; Kenney-Wallace, G. A. *Chem. Phys. Lett.* **1988**, *150*, 138; **1989**, *155*, 240.
(4) McMorrow, D.; Lotshaw, W. T. *Chem. Phys. Lett.* **1991**, *178*, 69.
(5) McMorrow, D.; Lotshaw, W. T. *J. Phys. Chem.* **1991**, *95*, 10395.
(6) Hattori, T.; Terasaki, A.; Kobayashi, T.; Wada, T.; Yamada, A.; Sasabe, H. *J. Chem. Phys.* **1991**, *95*, 937.
(7) Chang, Y. J.; Castner, Jr., E. W. *J. Chem. Phys.* **1993**, *99*, 113.
(8) Chang, Y. J.; Castner, Jr., E. W. *J. Chem. Phys.* **1993**, *99*, 7289.
(9) Ziegler, L. D.; Fan, R.; Desrosiers, A. E.; Scherer, N. F. *J. Chem. Phys.* **1994**, *100*, 1823.
(10) Cho, M.; Du, M.; Scherer, N. F.; Fleming, G. R.; Mukamel, S. *J. Chem. Phys.* **1994**, *99*, 2410.
(11) Deuel, H. P.; Cong, P.; Simon, J. P. *J. Phys. Chem.* **1994**, *98*, 12600.
(12) Chang, Y. J.; Castner, Jr., E. W. *J. Phys. Chem.* **1994**, *98*, 9712.
(13) Castner, Jr., E. W.; Chang, Y. J.; Chu, Y. C.; Walrafen, G. E. *J. Chem. Phys.* **1995**, *102*, 653.
(14) Lotshaw, W. T.; McMorrow, D.; Thantu, N.; Melinger, J. S.; Kitchenham, R. *J. Raman Spectrosc.* **1995**, *26*, 571.
(15) Deuel, H. P.; Cong, P.; Simon, J. P. *J. Raman Spectrosc.* **1995**, *26*, 523.
(16) McMorrow, D.; Thantu, N.; Melinger, J. S.; Kim, S. K.; Lotshaw, W. T. *J. Phys. Chem.* **1996**, *100*, 10389.
(17) Palese, S.; Mukamel, S.; Miller, R. J. D.; Lotshaw, W. T. *J. Phys. Chem.* **1996**, *100*, 10380.
(18) Cong, P.; Simon, J. D.; She, C. Y. *J. Chem. Phys.* **1996**, *104*, 962.
(19) Back, R.; Kenney-Wallace, G. A.; Lotshaw, W. T.; McMorrow, D. *Chem. Phys. Lett.* **1992**, *191*, 423.
(20) Cho, M.; Rosenthal, S. J.; Scherer, N. F.; Ziegler, L. D.; Fleming, G. R. *J. Chem. Phys.* **1992**, *96*, 5033.
(21) Vohringer, P.; Arnett, D. C.; Westervelt, R. A.; Feldstein, M. J.; Scherer, N. F. *J. Chem. Phys.* **1995**, *102*, 4027.
(22) Ruhman, S.; Joly, A. G.; Nelson, K. A. *J. Chem. Phys.* **1987**, *86*, 6563. Ruhman, S.; Joly, A. G.; Nelson, K. A. *IEEE J. Quantum Electron.* **1988**, *24*, 460.
(23) Pollard, W. T.; Lee, S.-Y.; Mathies, R. A. *J. Chem. Phys.* **1990**, *92*, 4012.
(24) Stock, G.; Domke, W. *Phys. Rev.* A, **1992**, *45*, 3032.
(25) Cong, P.; Yan, Y. J.; Deuel, H. P.; Simon, J. D. *J. Chem. Phys.* **1994**, *100*, 7855.
(26) Zhu, L.; Li, P.; Huang, M.; Sage, J. T.; Champion, P. M. *Phys. Rev. Lett.* **1994**, 72.
(27) Chachisvilis, M.; Fidder, H.; Sundstrom, V. *Chem. Phys. Lett.* **1995**, *234*, 141.
(28) Chachisvilis, M.; Fidder, H.; Pullerits, T.; Sundstrom, V. *J. Raman Spectrosc.* **1995**, *26*, 513.
(29) Vohringer, P.; Westervelt, R. A.; Yang, T.-S.; Arnett, D. C.; Feldstein, M. J.; Scherer, N. F. *J. Raman Spectrosc.* **1995**, *26*, 535.
(30) Zhu, L.; Wang, W.; Sage, J. T.; Champion, P. M. *J. Raman Spectrosc.* **1995**, *26*, 527.
(31) Eesley, G. L.; Levenson, M. D.; Tolles, W. M. IEEE *J. Quantum Electron. QE* **1978**, *14*, 45. Levenson, M. D.; Eesley, G. L. *Appl. Phys.* **1979**, *19*, 1.
(32) Yan, Y.; Mukamel, S. *Phys. Rev.* A **1990**, *41*, 6485.
(33) Walsh, A. M.; Loring, R. F. *Chem. Phys. Lett.* **1989**, *160*, 299.
(34) Herzberg, G. *Molecular Spectra and Molecular Structure*; Van Nostrand: New York, 1945; Vol. II.
(35) Scherer, N., (private communication).
(36) McMorrow, D.; Lotshaw, W. T. *Chem. Phys. Lett.* **1990**, *174*, 85.
(37) Tanimura, Y.; Mukamel, S. *J. Chem. Phys.* **1993**, *99*, 9496.
(38) Cho, M.; Fleming, G. R. *J. Phys. Chem.* **1994**, *98*, 3478.